IOP Publishing Journal of Physics D: Applied Physics
J. Phys. D: Appl. Phys. **50** (2017) 455102 (9pp) https://doi.org/10.1088/1361-6463/aa88f6

Morphology control, electronic properties and evolution of light emission in faceted indium oxide structures

Hassan Ouacha[1], Ulf Kleineberg[2] and Hamad Albrithen[1,3,4]

[1] King Abdullah Institute for Nanotechnology, King Saud University, PO Box 2455, Riyadh 11451, Saudi Arabia
[2] Faculty of Physics, Ludwig Maximilian University of Munich, 85748 Garching, Germany
[3] Physics and Astronomy Department, King Saud University, Riyadh 11451, Saudi Arabia
[4] National Center for Nanotechnology, KACST, Riyadh, Saudi Arabia

E-mail: houacha@ksu.edu.sa (Hassan Ouacha)

Received 19 February 2017, revised 23 August 2017
Accepted for publication 29 August 2017
Published 20 October 2017

Abstract

In_2O_3 micro-rods consisting of In_2O_3 rods with pyramid-like shape structures on top were synthesized on Au-catalyzed quartz substrates, via a vapor–solid process by a controlled vapor transport method. It was found that the Au catalyst and vapor–solid mechanism played an important role in the growth process and the growth phenomena in these structures were found to be in agreement with the preferential growth directions. The morphology and the structural evolution of the structure were successfully controlled and examined during the synthesis process. The controlled synthesis has made it possible for the In_2O_3 pyramid to be obtained either as an individual structure or as a cap on top of an In_2O_3 rod. In_2O_3 pyramids and In_2O_3 micro-rods were prepared at 900 and 1000 °C, respectively, and their electronic and room-temperature photoluminescence properties have been investigated. Current–voltage measurements were performed on a single In_2O_3 micro-rod in the temperature range 300–400 K and good quality ohmic contacts were obtained. Furthermore, the conductance of the In_2O_3 micro-rod has been found to increase slightly with increasing temperature, as revealed by temperature-dependent measurements. Photoluminescence measurements showed that In_2O_3 pyramids exhibited a UV luminescence band centered at 366 nm, while light emissions covering nearly the whole blue region have been observed in In_2O_3 micro-rods. The present work will enrich synthesis science and strongly indicates that processing conditions, as well as the morphology evolution control, are effective ways of fabricating In_2O_3-based tunable light-emitting devices. Furthermore, the faceted In_2O_3 microcrystal synthesized in this work may be promoted as pyramidal In_2O_3 microcavity, due to its unique shape that may allow multiple internal reflections of light at the titled pyramid facets.

Keywords: chemical vapor deposition, vapor–solid growth, photoluminescence, optical resonator, synthesis control, In_2O_3 pyramids and micro-rods, electronic properties

(Some figures may appear in colour only in the online journal)

1. Introduction

Indium oxide (In_2O_3) is an important wide bandgap semiconductor and has been studied for advanced applications in electronic, optoelectronic, photo-detectors, memory devices and high sensitivity sensors [1–5]. Different methods have been used to synthesize In_2O_3 micro/nanostructures such as thermal evaporation [6], sol-gel deposition [7], chemical vapor deposition (CVD) [8] and laser ablation [9]. While In_2O_3 micro/nanowires are extensively studied, investigations on three-dimensional (3D) In_2O_3 structures having different morphologies and cross-sections are still limited. Furthermore, it has

Table 1. Experimental condition for experiment I and II.

Experiment	Structure	Growth temperature (°C)	Ar/O_2 mixture	Ar/O_2 flow (sccm)	Pressure (Pa)	In weight (g)
I	In_2O_3 pyramids	900	9:1	50	86	0.2
II	In_2O_3 micro-rods	1000	9:1	50	86	7

been reported that the practical performances of In_2O_3 are relative to its morphology and size, which in turn depends on the preparation conditions [10–15]. Consequently, efforts have been devoted to synthesizing In_2O_3 materials with different characteristics [10–15], aiming at exploiting their potential applications. The search for well-defined In_2O_3 structures with different morphologies and different structural shapes on top will greatly promote this material for the development of miniature devices and fundamental physics research. Especially, In_2O_3 polyhedrons are of interest in optical applications, due to their vertices and faceted shapes, and have been studied as vertical Fabry–Perot resonators [16, 17]. Optical resonators-based faceted In_2O_3 structures have attracted great attention and have been the focus of studies in recent years [18, 19]. In_2O_3 microwire cavities with irregular hexagonal cross section have shown optical resonant modes in the visible spectral range [18]. In_2O_3 octahedra were studied as optical resonators and bow-tie modes were observed at room temperature by using the spatially resolved spectroscopic technique [19]. These studies indicated that 3D resonators can provide real light confinement in all three spatial dimensions, thus minimizing losses, and In_2O_3 optical resonators may be good candidates for the development of novel cavity-based optical devices. Moreover, there is a lack of reporting on direct evidence of morphological control and evolution in In_2O_3 rods with structural shapes on top during the fabrication process, especially the synthesis of In_2O_3 pyramid as an individual structure, as well as a cap on top of an In_2O_3 rod and its effect on the photoluminescence (PL) performance.

In this work, we report the synthesis of In_2O_3 rods with In_2O_3 pyramids on top by a Au-catalyzed CVD process and carefully analyze the growth mechanism of these structures by examining the morphology evolution of the structures during the growth. We also report a way to control the growth process to synthesize the In_2O_3 pyramid, both as an individual structure and as a cap on top of the In_2O_3 rod in a one-step growth synthesis. The electronic properties and the room-temperature PL characteristics of as-grown In_2O_3 pyramids and In_2O_3 micro-rods resulting from such a morphology-controlled synthesis are discussed. A potential application of these faceted In_2O_3 pyramids as 3D microcavities is proposed. Throughout this paper, we call the In_2O_3 micro-rod the full structure that consists of both In_2O_3 rod and In_2O_3 pyramid on top.

2. Experimental section

In_2O_3 pyramids and In_2O_3 micro-rods were synthesized by a Au-catalyzed CVD process using indium metal and oxygen vapor as source materials. High purity (99.995%) indium metal pellets were loaded into a ceramic boat and positioned at the center of a quartz tube inside a furnace. The furnace is equipped with a rotary vacuum pump, argon/oxygen gas mixture source, and a mass flow controller. Prior to the growth, an electron-beam evaporator was used to deposit a 2 nm gold film on a quartz substrate. The substrate was mounted in a vertical position at a height of 10 mm from the bottom horizontal plane of the boat and facing the gas mixture flow. Before heating, the quartz tube was evacuated to a base pressure below 0.1 Pa and then filled with an argon/oxygen gas mixture ($Ar:O_2 = 9:1$) at a rate of 50 sccm. Argon was used as the carrier gas. Two experiments have been conducted to synthesize the In_2O_3 products. In experiment I, 0.2 g of indium was used and the quartz tube was heated to 900 °C at a heating rate of 31 °C min^{-1} and kept at this temperature for different growth times under the constant flow of Ar/O_2 gas mixture. During the growth, the process pressure inside the tube was maintained at 86 Pa. In experiment II, indium with weight in the range of 0.5 to 7 g was used, the growth temperature was set to 1000 °C and the quartz tube was kept at this temperature for different growth times. Other experimental conditions were kept unchanged. When the growth temperature was chosen to be below 900 °C, only In_2O_3 islands were found. The parameters for each experiment are summarized in table 1. In each experiment, the synthesis process was terminated at the chosen growth time to examine the morphology evolution of the resultant structure and understand its growth mechanism. When the setting growth time was up, the furnace was turned off and cooled down to room temperature naturally. For safety reasons, it was only permitted to open the furnace and retrieve the sample from the quartz tube when furnace temperature was below 150 °C. The samples prepared in experiment I and experiment II were then collected after being annealed inside the furnace after growth, for 2 h and 3 h respectively. At the end of the process, a thick yellow layer was found deposited onto the substrate. The same synthesis processes were performed three times to confirm the reproducibility of the growth phenomena.

The morphology of the product was investigated using field emission scanning electron microscopy (FE-SEM S-4800) operating at 15 kV. The crystalline phase identification was conducted by an x-ray diffraction (XRD) system in the 2θ range from 10° to 90° at a scanning rate of 0.1° per 10 s using an x-ray diffractometer (Rigaku) with CuKα radiation ($\lambda = 1.54$ Å). The surface chemistry was examined by x-ray photoelectron spectroscopy (XPS) using PHI, 5600ci (Eden Prarie, MN) with a monochromatic aluminum x-ray source (1487 eV). The absorbance spectrum was taken at room temperature using an UV–VIS–NIR-spectrophotometer. To investigate the electronic properties of the In_2O_3 micro-rods, the grown structures were first scratched off from the substrate using a scalpel. A few drops of In_2O_3 structures-suspended in ethanol were poured onto an oxidized Si substrate equipped

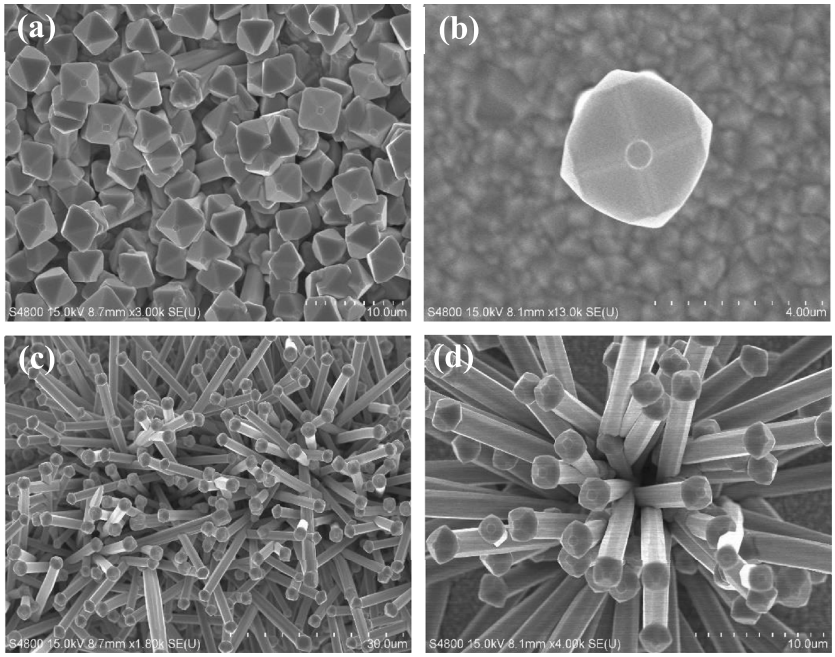

Figure 1. SEM images of the as-fabricated In_2O_3 pyramids and In_2O_3 micro-rods. (a) Large scale growth of In_2O_3 pyramids. (b) Top view image of an individual In_2O_3 pyramid. (c) Large scale growth of In_2O_3 micro-rods. (d) High-magnification image of In_2O_3 micro-rods.

with a large array of comb-shaped microelectrodes patterned by electron beam lithography. The microelectrodes were fabricated by thermal evaporation of Cr (20 nm)/Au (50 nm). Current–voltage (I–V) measurements were performed in the temperature range 300–400 K using a probe station equipped with a sample heater and temperature controller. PL spectrum was measured at room temperature in the range 320–490 nm in a spectrofluorophotometer with a Xe lamp using excitation at 300 nm (4.13 eV).

3. Results and discussion

The general morphologies of the as-prepared In_2O_3 pyramids and In_2O_3 micro-rods are shown in figure 1.

Figure 1(a) shows large scale growth of In_2O_3 pyramids as a product of experiment I. A typical In_2O_3 pyramid is shown in figure 1(b). The pyramid is found to have four equilateral triangles and a nearly square base with a diameter of 3.6 μm. These four facets meet at a cone that has a circular base with a diameter of 640 nm. SEM images of In_2O_3 micro-rods, as a result of experiment II, are shown in figures 1(c) and (d). The typical morphology of the In_2O_3 micro-rod reveals that the structure consists of both an In_2O_3 rod with a diameter of around 1.2 μm and an In_2O_3 pyramid on top. It is found that these In_2O_3 micro-rods can reach a length in a range of 10–20 μm depending on the amount of the supplied indium material source.

Structural characterization of as-grown In_2O_3 products was conducted with XRD. Figures 2(a) and (b) show the XRD pattern of In_2O_3 pyramids and In_2O_3 micro-rods, respectively.

All the sharp XRD diffraction peaks can be indexed to a body-centered cubic structure with lattice constant of $a = 10.10$ Å–10.11 Å in agreement with the standard value

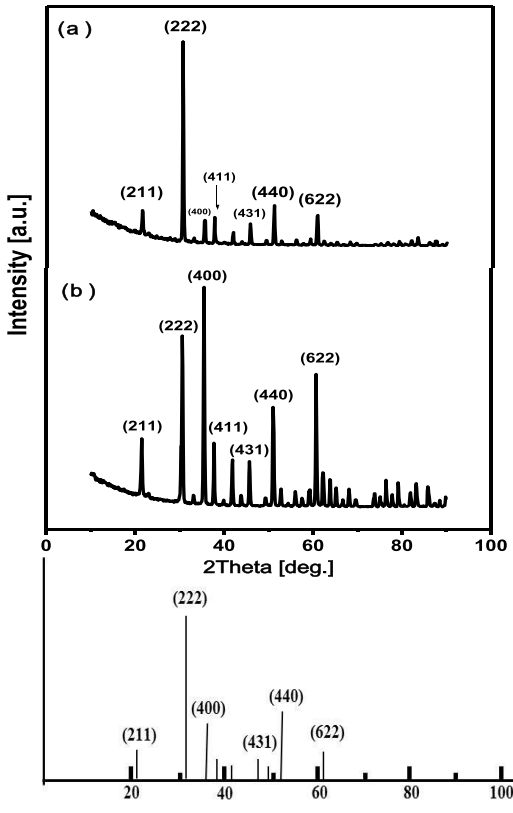

Figure 2. XRD spectra of the as-grown In_2O_3 (a) pyramids and (b) micro-rods. The inset of the bottom shows the line spectrum of the bulk In_2O_3 powder (JCPDS No. 89-4595).

for bulk cubic-In_2O_3 ($a = 10.12$ Å), (JCPDS No. 89-4595). It is known that the ratio $I_{(222)}/I_{(400)}$ called the crystal quality parameter [20] is about 3 for the bulk In_2O_3 powder (inset of the bottom of figure 2). The ratio is found to be around 8.25

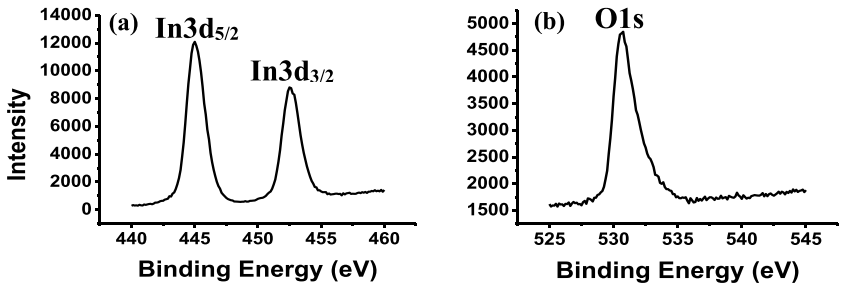

Figure 3. XPS spectra for (a) indium 3d and (b) oxygen 1s obtained from In_2O_3 pyramids and In_2O_3 micro-rods.

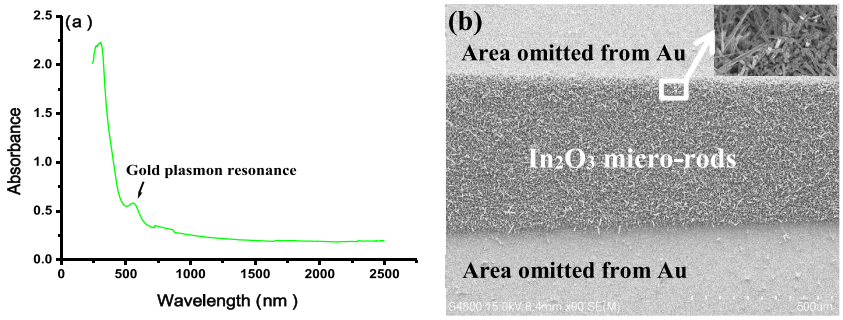

Figure 4. (a) Absorbance spectrum as a function of wavelength for In_2O_3 micro-rods with position of gold plasmon peak at 556 nm. (b) Areas of substrate omitted from Au show no growth of In_2O_3 micro-rods; the inset is a zoomed-in image of the area marked with a square showing growth of In_2O_3 micro-rods.

for In_2O_3 pyramids grown at 900 °C, as shown is figure 2(a). This indicates that the In_2O_3 pyramids are growing in the (1 1 1) direction and have a characteristic shape of the In_2O_3 crystal parallel to the (1 1 1) direction [19]. When the growth temperature is increased to 1000 °C, the ratio $I_{(222)}/I_{(400)}$ for In_2O_3 micro-rods is found to decrease compared to that of the bulk In_2O_3 powder and found to be 0.75. Since the increase of their density in the sample is accompanied by an increase in the (4 0 0) peak intensity, it is suggested that the In_2O_3 micro-rods are growing along the (1 0 0) direction. A similar (1 0 0) growth direction was found for In_2O_3 nanobelts [21].

The surface composition of the obtained In_2O_3 structures was verified by the XPS technique. Figures 3(a) and (b) show the XPS spectra for indium (3d) and oxygen (1s) from In_2O_3 pyramids and In_2O_3 micro-rods. The In3d core level shape and peak positions (445 and 452.5 eV for $In3d_{5/2}$ and $3d_{3/2}$, respectively) are found to be consistent with those of In_2O_3 [22].

The O1s peak displays a contribution at bending energy, ranging from 529.5 to 533.5 eV with a peak position at 530.75 eV, which can be assigned to the lattice oxygen in crystalline In_2O_3 [23]. However, the Au4f core level was not evident and no Au was detected in all samples, which indicates that the percentage of Au in indium is below its detection limit by XPS [24].

To discuss the growth mechanisms associated with the fabrication of In_2O_3 pyramids and In_2O_3 micro-rods, SEM observation revealed that the top of the structures does not contain any particle, as would be in the case of a vapor–liquid–solid (VLS) process often reported as the growth mechanism of Au-catalyzed In_2O_3 1D-structures [25]. Since XPS and SEM cannot reveal, in our case, information about the gold catalyst, we have used optical measurement to detect the presence of Au particles through plasmon resonance. Figure 4(a) shows the absorbance spectrum as a function of wavelength of In_2O_3 micro-rods naturally grown on quartz substrate. A similar spectrum was found for In_2O_3 pyramids.

It is known that the position of plasmon peak associated with gold particles depends on the shape and size of the particles and can be precisely controlled by the applied photon energy during growth [26]. The absorbance spectrum shows a clear peak at 556 nm, which can be attributed to the plasmon resonance of gold particles [26] and indicates the presence of Au in our structures. Furthermore, to show that a Au catalyst is necessary for the synthesis of our In_2O_3 structures, areas in some substrates were deliberately omitted from Au and we observed that no In_2O_3 growth occurred in any of the non-Au coated regions of the substrate, as shown in figure 4(b). The belt-like shape represents the Au-coated area of the substrate where large-scale growth of In_2O_3 micro-rods took place. The inset of figure 4(b) shows a zoomed-in image of the area marked with a square. Considering the results shown in figures 4(a) and (b), the absence of a Au particle at the top of the In_2O_3 pyramid and the non-detection of Au materials by XPS, it is suggested that Au may have been incorporated into In_2O_3 during growth or the Au residing at the base of the structure [27, 28]. Another possibility could be that Au stayed at the neck position below the top pyramid structure in the In_2O_3 micro-rod. Based on the results above, the growth mechanism responsible for the growth of our structures cannot be explained by the well-known VLS process.

To elucidate the growth mechanism of In_2O_3 pyramids and In_2O_3 micro-rods, the structural evolution of these products was carefully examined step by step during the synthesis process, as shown in figure 5. The setting growth time of

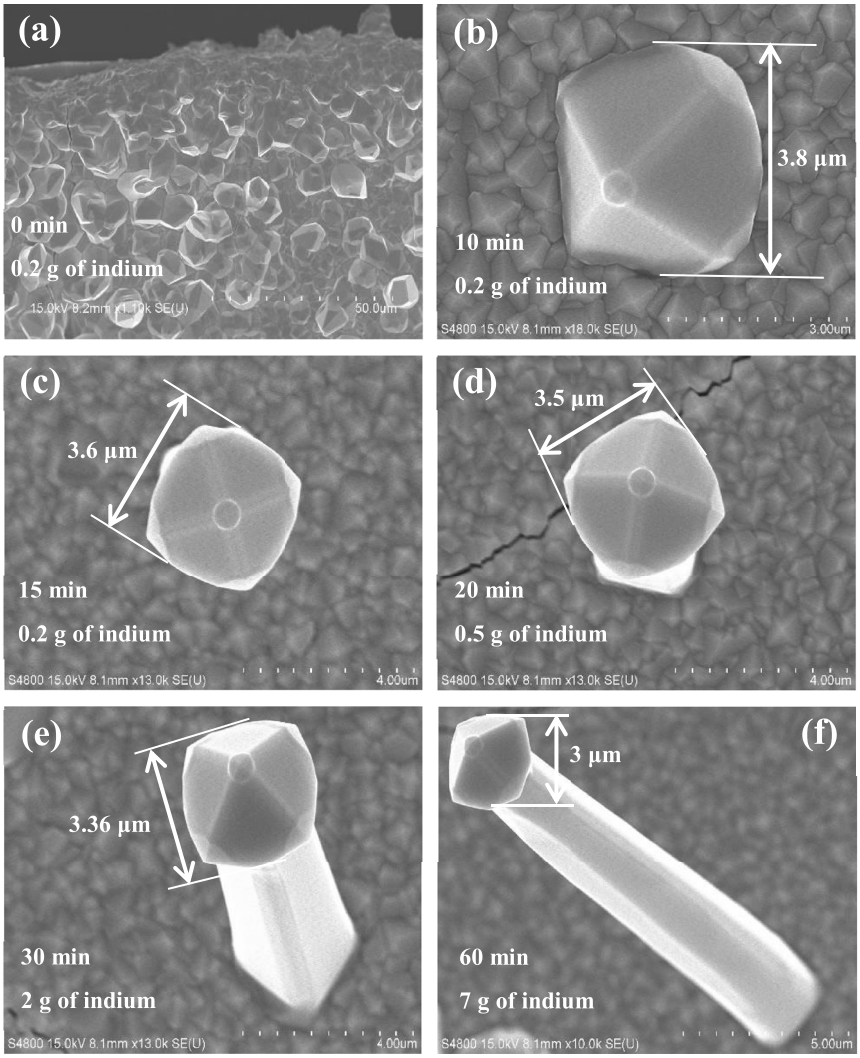

Figure 5. SEM images depicting the structural evolution of the In_2O_3 pyramid and the In_2O_3 micro-rod. (a)–(c) In_2O_3 pyramid synthesized at 900 °C at different growth times using 0.2 g of indium. (d)–(f) In_2O_3 micro-rod synthesized at 1000 °C at different growth times and indium weights.

0 min refers to turning off the furnace immediately after the set temperature is reached. In experiment I and at a growth time of 0 min, the Au film split into Au particles during the temperature increase. These Au particles served as nucleation sites for indium vapor produced at temperatures above the melting point of indium (156–157 °C). The indium atoms stuck to the Au catalyzed regions and indium-rich particles formed on the substrate. As Ar:O_2 gas mixture is continuously supplied, these particles can agglomerate during the temperature increase and form a group of In_2O_3 irregular structures, as shown in figure 5(a). Indium inside these particles would re-evaporate and be adsorbed on the structure surface to maintain, together with the incoming indium and oxygen species from vapor phase, the growth of the structure. As the growth time is increased to 10 min (figure 5(b)), and while the reaction went on, the structure provided further preferential accommodation sites for incoming indium that might react with oxygen from the argon/oxygen gas mixture source and formed In/In_2O_3 composite. The growth at this stage can be ascribed to the surface energy of crystallographic planes where preferential adsorption of In/O species on some of these special planes of In_2O_3 takes place, the so-called selective vapor–solid (VS) growth mechanism. It is known that in single crystal growth, the crystal morphology evolution is governed by decreasing the surface energy. The growth progressed to reduce the surface energy of the structure and the plane with the slowest growth rate would appear so that the In_2O_3 (1 1 1) facets would be formed ultimately, as shown in figure 5(b).

The obtained In_2O_3 pyramid with a base diameter of 3.8 μm is clearly faceted by low-index planes (1 1 1) in agreement with previous reports on the growth behavior of In_2O_3 structures suggesting that surface energy of (1 1 1) planes is lower than that of other low-index In_2O_3 planes [29, 30]. When the growth time is increased to 15 min, the selective VS growth reached saturation and the four facets of the In_2O_3 pyramid have been found to have the same growth rate resulting in the formation of a full symmetry form of the structure with a base diameter of 3.6 μm lying over the square (4 0 0) bottom plane, as shown in figure 5(c). Due to the VS growth saturation, the morphology and size of the In_2O_3 pyramid did not change when a longer growth time and more indium weight was applied at 900 °C. Furthermore, no growth of In_2O_3 rod

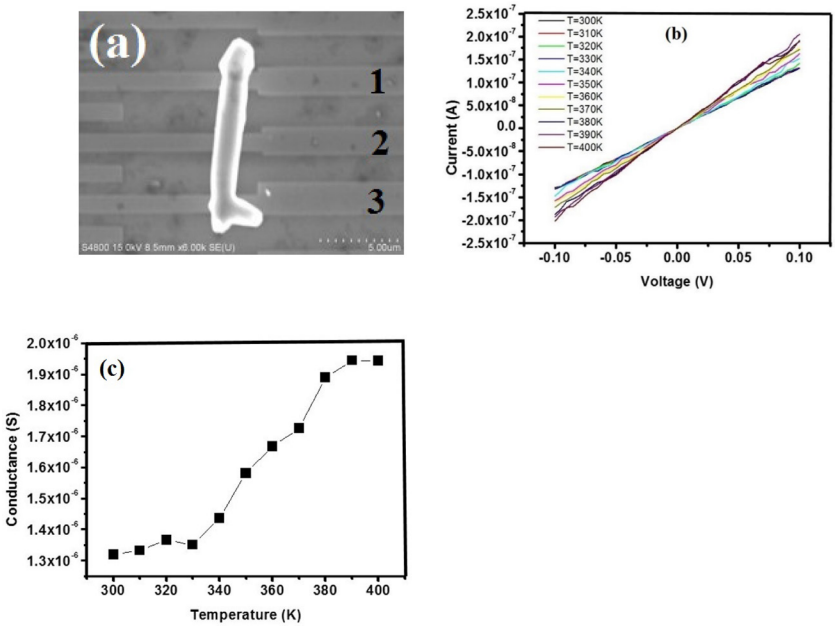

Figure 6. Electrical measurements on an individual In_2O_3 micro-rod. (a) In_2O_3 micro-rod attached to microelectrodes. (b) *I*–*V* curves recorded at different temperatures from 300 to 400 K. (c) Conductance as a function of temperature.

underneath the In_2O_3 pyramid was observed at this temperature. This is in agreement with previous studies reporting the growth of one-dimensional (1D) In_2O_3 structures by a vapor deposition technique, similar to our deposition method, at an elevated growth temperature of 950 °C [31]. Other researchers have used temperatures as high as 1030 °C [32] and 1400 °C [33]. The growth can be brought to an end and characterization of the In_2O_3 pyramid structure shown in figure 5(c) can be performed for a wide range of applications. Keeping the same indium weight of 0.2 g and applying a temperature of 1000 °C did not favor the start of the In_2O_3 rods growth, because the indium material amount was just enough to synthesize In_2O_3 pyramids. Therefore, both indium weight and growth time were varied in experiment II to follow the evolution of the structure at the increased growth temperature of 1000 °C.

To elucidate the growth mechanism of the In_2O_3 rod, more indium weight was applied and the growth temperature was increased to 1000 °C. As a first step, the growth time was set to 20 min and the indium weight was adjusted to 0.5 g. For In_2O_3 with the bcc structure, the surface energy relationships among three low-index crystallographic planes should correspond to $\gamma\{1\,1\,1\} < \gamma\{1\,0\,0\} < \gamma\{1\,1\,0\}$ [29]. At higher temperatures, the saturated In_2O_3 pyramid shown in figure 5(c) drove the precipitation of the vapor components of the indium source material and the oxidized-indium at the bottom of the structure. The adsorbed species would transfer to the next lower energy site at the square (4 0 0) bottom plane to maintain the subsequent 1D growth along the [1 0 0] crystalline direction. As a result, the start of the 1D growth took place underneath the In_2O_3 pyramid and In_2O_3 rod with a length of about 0.8 μm was obtained, as shown in figure 5(d). Ensuring a continuous supply of vapor components to continue the 1D growth, In_2O_3 rods with lengths of about 4.6 and 11 μm were obtained respectively with indium weights of 2 g and 7 g, as shown in figures 5(e) and (f). As can be observed from figures 5(d)–(f), the In_2O_3 pyramid shown in figure 5(d) was subject to the annealing effect during the growth of In_2O_3 rod at 1000 °C. The base diameter of the In_2O_3 pyramid was reduced from 3.5 to 3 μm when the growth time was increased from 20 to 60 min, respectively. The trend was sustained at growth temperature of 900 °C, where the base diameter of the In_2O_3 pyramid was found to decrease from 3.8 to 3.6 μm when the growth time was increased from 10 to 15 min, as shown in figures 5(b) and (c), respectively. The slight reduction in the In_2O_3 pyramid size may be attributed to the continued heat induced by longer growth times at higher temperatures of 900 and 1000 °C. At these high temperatures, diffusion and evaporation of atoms at the edge of the structure may be stimulated, and, as a result, the base diameter of the In_2O_3 pyramid is reduced. Furthermore, the diameter of the rod increased slightly towards the bottom from 1 μm at the upper part to 1.2 μm at the bottom, as can be seen in figure 5(f). This can be attributed to the exposure of the lower portion of the rod to indium vapor for a longer time, while the diameter at the most upper part of the rod is confined by the circular bottom plane (1 0 0). From the data of figures 5(d)–(f), the diameter of the In_2O_3 rod did not vary much during the synthesis process and found to be in the range of 1–1.2 μm. The synthesis results show that the growth process of In_2O_3 rod underneath the In_2O_3 pyramid can be attributed to self-catalytic VS growth mechanism and the full structure, In_2O_3 micro-rod, can be prepared in a one-step growth synthesis.

To summarize the effect of the growth parameters on the morphology of our In_2O_3 products, In_2O_3 pyramid was fabricated at growth temperature of 900 °C as a first step and its shape and size were found to be growth time controlled. The morphology of the full In_2O_3 micro-rod structure (In_2O_3 rod with In_2O_3 pyramid on top) was found to be dependent on growth temperature where the In_2O_3 pyramid was fabricated during the temperature increase. At the growth temperature

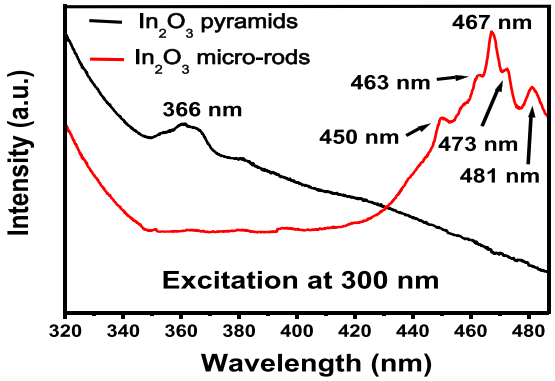

Figure 7. Photoluminescence spectra from In_2O_3 pyramids and In_2O_3 micro-rods at room temperature upon excitation at 300 nm.

of 1000 °C, the size of the top structure (In_2O_3 pyramid) was found to be dependent on the In_2O_3 rod growth time; meanwhile the size of the In_2O_3 rod was shown to be indium weight- and growth time-controlled.

Electrical conductance through these synthesized In_2O_3 micro-rods is relevant for electronic applications. Here, we employ an individual In_2O_3 micro-rod to investigate its conductance dependence on temperature. An SEM image of our device depicting a single In_2O_3 micro-rod connected to electrodes 1, 2 and 3 with gap spacing of 5 μm is shown in figure 6(a). Nevertheless, issues come into play when it comes to scratching the micro-rods or any other 1D structures off from the substrate and separating them. The structures are likely to break off and a few of them can be found to be useful for measurements. *I–V* measurements were performed between the electrodes 1–2, and similar results were obtained when measurements were taken between electrodes 2–3. As a part of the In_2O_3 micro-rod is connected to the conducting electrode 2, measurements between electrodes 1–3 were not performed. A similar strategy was used by Scheffler *et al* [34] to study the diameter-dependent conductance of tapered InAs nanowires by contacting multiple sections, with the same length, of an individual wire and the measurements were performed between adjacent electrodes. Figure 6(b) shows typical *I–V* characteristic curves taken from 300 to 400 K with a temperature *T* increment of 10 K. As depicted in this figure all curves exhibit linear *I–V* behavior and no Schottky-behaving Au–In_2O_3 contact was obtained in our device, showing that the fabrication process provides good metal–semiconductor ohmic contacts. Similar results were observed by Stern *et al* [35] when electron beam and optical lithography methods were used to fabricate ohmic contacts to nanowires and nanotubes. The linear behavior of *I–V* curves, in our case, can be explained by the flow of current from the entire Au–In_2O_3 contact area into the In_2O_3 micro-rod.

The temperature dependence of In_2O_3 micro-rod conductance is shown in figure 6(c). It is observed that the conductance increases from 1.32×10^{-6} S at 300 K (26 °C) to 1.95×10^{-6} S at 400 K (127 °C), in agreement with temperature dependence of semiconductor conductivity. This behavior is attributed to the increase of carrier density with increasing temperature, thus increasing the conductivity of In_2O_3 micro-rod. However, the conductance is not found to be sensitive to temperature changes in a range 300–330 K, as seen in figure 6(c). This may be due to the fact that the electrons in the valence band did not gain sufficient energy to escape from the confines of their atoms, and therefore the increase of temperature in this range was not enough to free more electrons to increase the conductivity of the In_2O_3 micro-rod.

While the electrical measurements on In_2O_3 nanowires and nanotubes are widely reported [36–39], there is a lack of reporting on the electronic properties of In_2O_3 rods with larger diameters, similar to our In_2O_3 micro-rods. Compared to our results, conductances in the range of 3.13×10^{-6} S–3.62×10^{-10} S were found for In_2O_3 nanowires with diameter of about 10 nm [38]. The conductance of a single ZnO nanowire was estimated to reach 0.41×10^{-6} S for an electrode spacing of 4 μm and an average nanowire diameter of 200 nm [40]. We note that although the conductance of our In_2O_3 micro-rod has increased with increasing temperature from 300 to 400 K (figure 6(c)), only a slight increase with less than one order of magnitude was observed. This indicates that these In_2O_3 micro-rods can maintain their room temperature electrical performance even at higher temperatures, which provides the possibility to use these structures in electronic devices operating at ambient temperatures and in which additional heating may be either needed for specific applications or unintentionally occurring as a result of overheating, for instance. These conductance measurements on In_2O_3 micro-rod thus complement the diameter-dependent conductance already reported for In_2O_3 nanowires, and emphasize that future efforts must address further investigations of temperature-dependent conductance of In_2O_3 1D-microstructures with large diameters.

The optical properties of the synthesized In_2O_3 structures were investigated by PL measurement. Figure 7 shows both the room-temperature PL spectrum of the as-prepared In_2O_3 pyramids and In_2O_3 micro-rods upon excitation at 300 nm (4.13 eV). As can be seen, In_2O_3 pyramids synthesized at 900 °C exhibited a luminescence band centered at 366 nm. A similar near UV emission at 338 nm has been observed in In_2O_3 crystals obtained by calcining the In_2S_3 clusters in air [41]. In our case, this UV PL peak can be attributed to near band edge emission around 3.4 eV from the wide bandgap In_2O_3 pyramids. The UV transition is believed to be due to the singly ionized oxygen vacancies in the structures, and the emission results from the radiative recombination of a photo-generated hole with an electron occupying this vacancy. Different PL results have been obtained by many groups. Liang *et al* observed PL peaks at 470 nm from In_2O_3 nanofibers [42], Li *et al* measured PL of the In_2O_3 nanotubes that exhibited emission of 593 nm [43], and Lee *et al* observed the PL peak at 637 nm from In_2O_3 films [44]. In these studies, the PL mechanism was mainly attributed to the effect of the oxygen deficiencies. When the In_2O_3 pyramids evolved to In_2O_3 micro-rods following the experimental conditions of experiment II at the higher growth temperature of 1000 °C, PL emission peaks are observed covering nearly the whole blue region (450–485 nm), as shown in figure 7. Predominant PL peaks with their maximum intensities centered at 467 and 481 nm, respectively, were detected. Because of the micro size of the

structure, these blue emissions cannot arise from a quantum confinement effect. Furthermore, these PL emissions (467 and 481 nm) would not come from the transition of excitons from the conduction band to the valence band of In_2O_3 micro-rods, since In_2O_3 is a semiconductor with a bandgap of around 3.6 eV (344 nm). Oxygen vacancies might be generated due to the rapid evaporation/oxidation process at 1000 °C and these emission peaks can be referred to trap state emissions, which may be due to these oxygen vacancies. In_2O_3 is known to possess electronic n-type properties and the reason is there are not sufficient oxygen atoms to catch the electrons released from indium atom, which make these electrons form the donor level. The oxygen vacancies can cause many localized states between the conduction and valence band. The blue emission would arise from these energy levels in the In_2O_3 micro-rods, so distinguishable PL peaks were also observed at 450, 463 and 473 nm, respectively.

As discussed above, In_2O_3 pyramids were subjected to the annealing effect during the growth of In_2O_3 rods at 1000 °C. The effect of this annealing process on the PL properties of the full structures, In_2O_3 micro-rods, is reflected by the extinction of the UV emission at 366 nm previously observed from In_2O_3 pyramids, as shown in figure 7. This may indicate that oxygen vacancies in In_2O_3 pyramids have been reduced, due to longer growth time of the In_2O_3 rods and pushed the donor level away from the conduction band. This has resulted in a shift of the UV PL peak toward the blue region. The shift of PL peak position from UV to the blue region (redshift) strongly indicates that the processing conditions, as well as the structural evolution control, are promising ways to tune the PL of In_2O_3 pyramids and In_2O_3 micro-rods. Such structures should have great potential for applications of In_2O_3-based tunable light-emitting devices.

Furthermore, 3D faceted structures have attracted much interest as optical resonators, providing real light confinement in all three spatial dimensions. In search of such 3D cavities, pyramidal resonators have recently been demonstrated to be promising candidates [45, 46]. Contrary to the traditional optical cavity in lasers, which consists of a Fabry–Perot (FP) resonator formed by two parallel mirrors and produces a standing-wave pattern within the cavity [47], the advantage of structures with multi- and non-parallel facets is that light can be confined by many boundaries. Relying on the retroreflector principle, the faceted In_2O_3 pyramids synthesized in this work may allow multiple internal reflections of light at the titled pyramid facets, thus minimizing losses. They may be promoted as pyramidal In_2O_3 microcavities and find many applications in developing 3D resonators.

4. Conclusions

The synthesis of In_2O_3 micro-rods by a controlled Au-catalyzed vapor transport method is shown. The morphology and the structural evolution of the structure are successfully controlled and examined during the synthesis process. In_2O_3 pyramids can be prepared either as individual structures or as caps on top of In_2O_3 rods. The growth process of In_2O_3 pyramids and In_2O_3 micro-rods can be attributed to catalyst-assisted and self-catalytic VS mechanisms, respectively. Current–voltage measurements are performed on a single In_2O_3 micro-rod and good quality ohmic contacts are obtained. From the temperature-dependent measurements, the conductance of the In_2O_3 micro-rod is found to increase slightly with increasing temperature from 300 to 400 K. A room–temperature PL study shows a UV-light emission in In_2O_3 pyramids, which might be related to the recombination of a photo-generated hole with an electron occupying singly ionized oxygen vacancy. The evolution of the structure from the In_2O_3 pyramid to In_2O_3 micro-rod causes a large redshift in the PL emission spectra. The results suggest that these In_2O_3 structures have the potential to be a UV and a blue light emitter and indicate that their preparation by a morphology-controlled synthesis is an effective way of fabricating In_2O_3-based tunable light-emitting devices. Due to its faceted shape, In_2O_3 pyramid may allow multiple internal reflections of light and should have great potential for applications such as in 3D resonators.

Acknowledgment

The authors extend their appreciation to the Deanship of Scientific Research at King Saud University for funding this work through research group no IRG14-07A.

References

[1] Li C, Fan W, Straus D A, Lei B, Asano S, Zhang D, Han J, Meyyappan M and Zhou C 2004 *J. Am. Chem. Soc* **126** 7750
[2] Li C, Curreli M, Lin H, Lei B, Ishikawa F N, Datar R, Cote R J, Thompson M E and Zhou C 2006 *J. Am. Chem. Soc* **127** 12484
[3] Nguyen P, Hou T N, Yamada T, Smith M K, Li J, Han J and Meyyappan M 2004 *Nano Lett.* **4** 651
[4] Kiriakidis G, Ouacha H, Katsarakis N, Galatsis K and Wlodarski W 2003 *Proc. SPIE* **5116** 84
[5] Kiriakidis G, Ouacha H and Katsarakis N 2003 *Rev. Adv. Mater. Sci.* **4** 32
[6] Wang Y, Yawei Li, Ke Yu and Zhu Z 2011 *J. Phys. D: Appl. Phys.* **44** 105301
[7] Cheng Z, Dong X, Pan Q, Zhang J and Dong X 2006 *Mater. Lett.* **60** 3137
[8] Kim H W, Kim N H and Lee C 2005 *Appl. Phys.* A **81** 1135
[9] Li C, Zhang D, Han S, Liu X, Tang T and Zhou C 2003 *Adv. Mater.* **15** 143
[10] Kuo C Y, Lu S Y and Wei T Y 2005 *J. Cryst. Growth* **285** 400
[11] Datta A, Panda S K, Ganguli D, Mishra P and Chaudhuri S 2007 *Cryst. Growth Des.* **7** 163
[12] Wang C, Chen D, Jiao X and Chen C 2007 *J. Phys. Chem.* C **11** 13398
[13] Wu P, Li Q, Zhao C X, Zhang D L, Chi L F and Xiao T 2008 *Appl. Surf. Sci.* **255** 3201
[14] Zhang L X, Zhang Y C and Zhang M 2009 *Mater. Chem. Phys.* **118** 223
[15] Huang Z, Chai C, Tan X, Wu J, Yuan A and Zhou Z 2007 *Mater. Lett.* **61** 5137
[16] Dong H, Sun H S, Sun L, Xie W, Zhou L, Shen X and Chen Z 2011 *Appl. Phys. Lett.* **98** 011913
[17] Wang Z L 2000 *J. Phys. Chem.* B **104** 1153

[18] Dong H, Liu Y, Sun S, Chen Z and Zhang L 2014 *J. Mater. Chem.* C **2** 8976
[19] Dong H, Sun L, Sun S, Xie W, Zhou L, Shen X and Chen Z 2010 *Appl. Phys. Lett* **97** 223114
[20] Gulen M, Yildirim G, Bal S, Varilci A, Belenli I and Oz M 2012 *J. Mater. Sci., Mater. Electron.* **24** 467
[21] Gao T and Wang T 2006 *J. Cryst. Growth* **290** 660
[22] Vomieroa A, Ferroni M, Natilec M M, Fischere T, Fize R, Mathure S and Sberveglieri G 2014 *Appl. Surf. Sci.* **323** 59
[23] Jo G, Hong W K, Maeng J, Kim T W, Wang G, Yoon A, Kwon S S, Song S and Lee T 2008 *Colloids Surf.* A **313–4** 308
[24] Shard A G 2014 *Surf. Interface Anal.* **46** 175
[25] Chen C J, Xu W L and Chern M Y 2007 *Adv. Mater.* **19** 3012
[26] Ouacha H, Hendrich C, Hubenthal F and Trager F 2005 *Appl. Phys.* B **81** 663
[27] Tai K, Sun K, Huang B and Dillon S J 2014 *Nanotechnology* **25** 145603
[28] Lee J M, Xia F, Nichols W T, Choi C and Park W I 2012 *Met. Mater. Int.* **18** 875
[29] Zhang K H, Walsh A, Catlow C R, Lazarov V K and Egdell R G 2010 *Nano Lett.* **10** 3740
[30] Hao Y, Meng G, Ye C and Zhang L 2005 *Cryst. Growth Des.* **5** 1617
[31] Zeng F, Zhang X, Wang J, Wang L and Zhang L 2004 *Nanotechnology* **15** 596
[32] Peng X S, Wang Y W, Zhang J, Wang X F, Zhao L X, Meng G W and Zhang L D 2002 *Appl. Phys.* A **74** 437
[33] Pan Z W, Dai Z R and Wang Z L 2001 *Science* **291** 1947
[34] Scheffler M, Nadj-Perge S, Kouwenhoven L P, Borgström M T and Bakkers P A M 2009 *J. Appl. Phys.* **106** 124303
[35] Stern E, Cheng G, Klemic J F, Broomfield E, Turner-Evans D, Li C, Zhou C and Reed M A 2006 *J. Vac. Sci. Technol.* B **24** 231
[36] Liu F, Bao M, Wang K L, Li C, Lei B and Zhou C 2005 *Appl. Phys. Lett.* **86** 213101
[37] An S, Park S, Ko H, Jin C, Lee W I and Lee C 2013 *J. Phys. Chem. Solids* **74** 979
[38] Li C, Zhang D, Han S, Liu X, Tang T, Lei B, Liu Z and Zhou C 2003 *Ann. NewYork Acad. Sci.* **1006** 104
[39] Liu H, Li J and Tan R 2017 *IEEE J. Electron Devices Soc.* **5** 141
[40] Bercu B, Geng W, Simonetti O, Kostcheev S, Sartel C, Sallet V, Lérondel G, Molinari M, Giraudet L and Couteau C 2013 *Nanotechnology* **24** 415202
[41] Zhang L X, Zhang Y C and Zhang M 2010 *Mater. Lett.* **64** 966
[42] Liang C, Meng G, Lei Y, Phillipp F and Zhang L 2001 *Adv. Mater.* **13** 1330
[43] Li Y, Bando Y and Golberg D 2003 *Adv. Mater.* **15** 581
[44] Lee M S, Choi W C, Kim E K, Kim C K and Min S K 1996 *Thin Solid Films* **279** 1
[45] Bartolome J, Cremades A and Piqueras J 2013 *J. Mater. Chem.* C **1** 6790
[46] Zhang X and Hu E L 2016 *Appl. Phys. Lett.* **109** 081101
[47] Bhowmik A K 2000 *Appl. Opt.* **39** 3071